DOI: 10.1002/ejic.200801138

Diphenic Acid-Based Cobalt(II) Complexes: Trinuclear and Double-Helical Structures

Iurii L. Malaestean,[a] Manfred Speldrich,[a] Svetlana G. Baca,[b] Arkady Ellern,[c] Helmut Schilder,[a] and Paul Kögerler*[a]

Keywords: Cobalt / Carboxylate ligands / Coordination polymers / Magnetic properties / N ligands

The linear trinuclear complex $[Co_3(dpa)_2(Hdpa)_2(1\text{-MeIm})_2(H_2O)_2]$ (**1**) and the two-dimensional coordination polymer $[Co_2(dpa)_2(pyz)]_n$ (**2**; H_2dpa = diphenic acid, 1-MeIm = 1-methylimidazole, pyz = pyrazine) exemplify the versatile coordination chemistry of diphenic acid in conjunction with N-donor ligands. Complex **1** consists of a discrete arrangement of three Co^{II} atoms bridged by four diphenate ligands, whereas complex **2** contains a network of dinuclear Co^{II} units bridged by two diphenate ligands to form double-helical chains, which are further connected via pyrazine molecules into two-dimensional sheets. A magnetochemical analysis of these complexes reveals both strong ligand field effects on the Co^{II} ^4F free ion ground state and ferro- and antiferromagnetic exchange contributions mediated by the dpa ligands.

Introduction

Coordination polymers are currently being increasingly targeted due to their numerous nanotechnology and engineering applications in gas storage, separation, sensor technology, magnets, optoelectronics, energy conversation and storage, and catalysis.[1] Motivated by these technological applications, this area has developed rapidly over the last two decades, especially the field of metal-organic frameworks (MOFs), which has led to the development of concepts such as the use of supramolecular synthons. One exemplary approach to the design and synthesis of coordination polymers uses dicarboxylic acids as spacers between coordinated metal ions. The specific advantage of such spacers is the diversity of bonding modes of carboxylate groups − Porai-Koshits[2] has listed nineteen different coordination modes − which can lead to intriguing architectures and topologies.

In our recent work on the assembly of coordination polymers, we have synthesized a series of new cobalt(II), nickel(II), copper(II), and zinc(II) complexes using *o*-phthalic dicarboxylic acid.[3] The resulting coordination structures, which depend on the metal coordination geometry and the metal-to-ligand ratio chosen, exhibit diverse polymeric architectures. Herein we describe an extension of our studies on the construction of coordination polymers with benzene dicarboxylates by employing 2,2′-diphenyldicarboxylic acid (diphenic acid, H_2dpa). Deprotonated diphenic acid is a flexible ligand that can form a variety of coordination architectures with different dimensionalities. Recent examples include one-dimensional double-chain $[Cu(dpa)(H_2O)]_n$,[4] ladder-type double-chain $[Zn(dpa)(H_2O)]_n$,[5] and helical-chain $[Cu(dpa)(H_2O)_4]_n$[6] coordination polymers, as well as helical-chain $[M(dpa)(H_2O)_8]_n$ (M = Co^{II}, Ni^{II}[7]) and butterfly-like chain $[Co_3(dpa)_{2.5}(OH)(H_2O)_2]_n$[8] coordination polymers. Several new lanthanide complexes with the composition $[Ln(dpa)_3(H_2O)_2]_n$,[9,10] which form zigzag chains, have also been obtained, as have one-, two-, and three-dimensional coordination polymers of zinc(II), copper(II), cadmium(II), nickel(II) and cobalt(II) diphenates containing additional N-containing ligands.[5,6,11–13] Note, for example, that the coordination polymer $\{[Zn_2(dpa)_2(bpp)_2(H_2O)_3]\cdot 0.75H_2O\}_n$[14] exhibits an extended tetrazinc metallacrown architecture bridged by 1,3-bis(4-pyridyl)propane (bpp) linkers into two-dimensional networks. A very interesting three-dimensional pillared framework, $\{[Cd_2(dpa)(pya)]_6(pya)_6(dpe)_3\}_n$,[15] has been constructed from dodecanuclear cadmium macrocycles with 1,2-bis(4-pyridyl)ethylene (dpe) and isonicotinate (pya). Other dicarboxylic acids, such as terephthalic acid (bdc), have led to an unusual three-dimensional porous architecture constructed from trimetallic cluster helical chains connected by terephthalic ligands, namely $[Zn_3(dpa)_2(bdc)]_n$.[16] Discrete (molecular) diphenate complexes are usually dinuclear, such as the complexes found in the compounds $[Mn_2(dpa)_2(bpy)(H_2O)_5]\cdot 4H_2O$[17] and $[M_2(dpa)L_4](ClO_4)_2$[18] [M = Ni^{II}, Co^{II}, and Mn^{II}; L = diaminoethane,

[a] Institut für Anorganische Chemie, RWTH Aachen University, 52074 Aachen, Germany
E-mail: paul.koegerler@ac.rwth-aachen.de
[b] Institute of Chemistry, ASM, 2028 Chisinau, Moldova
[c] Department of Chemistry, Iowa State University, Ames, IA 50011, USA
Supporting information for this article is available on the WWW under http://www.eurjic.org/ or from the author.

1,2-diaminopropane, and 1,3-diaminopropane for Ni^{II} and Co^{II}; L = bpy (2,2′-bipyridyl), 5-NO_2-1,10-phenanthroline and 1,10-phenanthroline for Mn^{II}].

This paper describes the hydrothermal synthesis, crystal structures, and magnetic properties of both a larger discrete complex, namely the linear trinuclear cluster $[Co_3(dpa)_2(Hdpa)_2(1\text{-MeIm})_2(H_2O)_2]$ (**1**), and the new two-dimensional coordination polymer $[Co_2(dpa)_2(pyz)]_n$ (**2**; 1-MeIm = 1-methylimidazole, pyz = pyrazine).

Results and Discussion

Synthetic Methodology

A hydrothermal approach was used to synthesize both complexes in order to overcome solubility limitations in aqueous reaction solutions. The linear discrete carboxylate cluster **1** was prepared by the reaction of cobalt(II) acetate with diphenic acid in the presence of 1-MeIm, whereas the polymeric complex **2** was synthesized by the interaction of cobalt(II) acetate, diphenic acid, and NaOH with pyrazine as a bridging ligand.

Structural Description of $[Co_3(dpa)_2(Hdpa)_2(1\text{-MeIm})_2(H_2O)_2]$ (1)

Single crystal X-ray diffraction analysis shows that complex **1** crystallizes in the monoclinic space group $P2_1/c$ and comprises a linear arrangement of three Co^{II} centers bridged by four diphenate ligands. The structure of complex **1** is displayed in Figure 1 and selected bonds and angles are listed in Table 1 (see Figure S1 for a packing diagram). The central Co1 site, which is located on the crystallographic inversion center, is coordinated by six carboxylate oxo centers from four different diphenate ligands, with Co–O bond lengths in the range 2.037(1)–2.136(1) Å, and thus adopts a distorted octahedral O_6 environment. The two terminal cobalt centers (Co2 and Co2A) are in a distorted square-pyramidal NO_4 environment, coordinated by four oxygen centers − three oxygen carboxylate positions from three diphenate ligands [Co–O distances range from 1.967(1) to 2.343(2) Å] and one water ligand [Co–O_w 1.985(2) Å] − and a nitrogen atom from a 1-MeIm molecule [Co–N 2.055(2) Å]. The Co···Co separation in the cluster is 3.217(5) Å, with a shortest intermolecular Co···Co distance of 5.712 Å. The Co···Co intracluster and intercluster separations are both shorter than those reported in analogous linear trinuclear cobalt(II) carboxylate complexes such as $[Co_3(quin)_2(PhCO_2)_6]$ and $[Co_3(quin)_2(phcina)_6]$, (quin = quinoline; phcina = phenylcinnamate),[19] where the Co···Co separations are 3.57 and 7.37 Å, respectively. Two diphenate groups act as tetradentate ligands and form bridges between a pair of cobalt centers in the usual μ_2-1,3 coordination fashion. The other two diphenate ligands function as bidentate ligands where only one carboxylate group bridges two metal centers (Co1 and Co2/Co2A) in a μ_2-η^2 coordination mode, while the second carboxylic group remains uncoordinated and forms O–H···O-type hydrogen bond networks with oxygen sites of carboxylate groups of adjacent complex molecules in the solid state [O4–H4B···O9(–*x* + 1, *y* + 1/2, –*z* + 1/2) 2.633(2) Å]. The terminal water ligands form two types of hydrogen-bond interactions: an intramolecular hydrogen bond with the carboxylate atom O9 [O6w–H6B···O9(–*x*+1, –*y*, –*z*) 2.659(2) Å] and an intermolecular hydrogen bond of 2.643(2) Å with the carboxylate O7(–*x* + 2, –*y*, –*z*) atom from an adjacent complex (Figure 2).

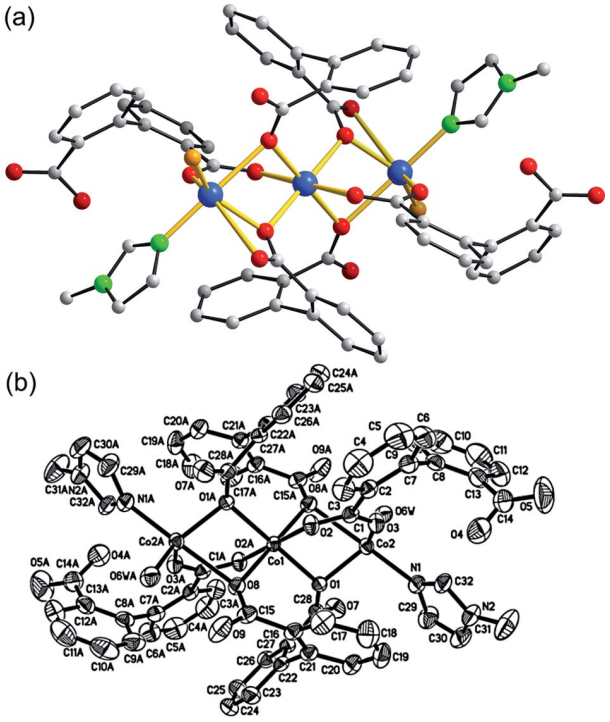

Figure 1. (a) Ball-and-stick representation of the $\{Co_3\}$ cluster **1**. Hydrogen atoms have been omitted for clarity in this and subsequent figures. Color code: Co: blue; O: red; O(H_2): orange; C: gray; N: green. Coordination environments are highlighted by yellow bonds. (b) Corresponding ORTEP plot with numbered positions ("A" denotes the symmetry operation –*x* + 1, –*y*, –*z*).

Table 1. Selected bond lengths [Å] and angles [°] in complex **1**.[a]

Co1–O1	2.114(1)	Co2–O3	1.967(1)
Co1–O2^i	2.037(1)	Co2–O6w	1.985(2)
Co1–O8	2.136(1)	Co2–O1	2.001(1)
Co2–N1	2.055(2)	Co2–O8^i	2.343(2)
O1^i–Co1–O8^i	101.99(5)	O1–Co2–N1	102.59(7)
O8–Co1–O8^i	180.0(1)	N1–Co2–O8^i	175.64(6)
O2^i–Co1–O2	180.0(1)	O3–Co2–O6w	119.25(7)
O2^i–Co1–O1	86.63(6)	O1–Co1–O8^i	78.01(5)
O2–Co1–O1	93.37(6)	O3–Co2–O1	98.64(6)
O2–Co1–O1^i	90.73(7)	O6w–Co2–O1	135.53(6)
O1–Co1–O1^i	180.00(8)	O3–Co2–N1	86.63(6)
O2^i–Co1–O8	88.55(6)	O6w–Co2–N1	99.49(7)
O2–Co1–O8	91.45(6)	O3–Co2–O8^i	85.70(6)
O1–Co1–O8	101.99(5)	O6–Co2–O8^i	84.45(6)
O1^i–Co1–O8	78.01(5)	O1–Co2–O8^i	75.54(5)
O2^i–Co1–O8^i	91.45(6)	O2–Co1–O8^i	88.55(6)

[a] Symmetry transformations used to generate equivalent atoms *i*: –*x* + 1, –*y*, –*z*.

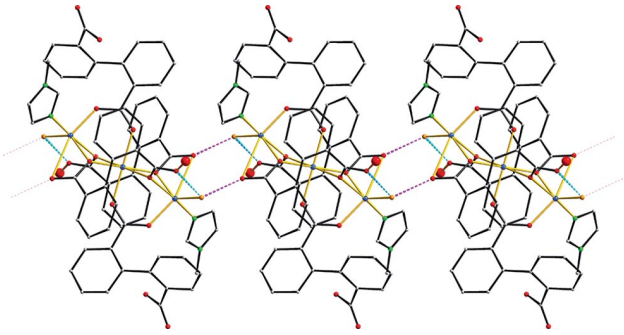

Figure 2. Hydrogen bonds connect the linear $\{Co_3\}$ complexes into chains in the solid-state structure of compound **1**. Intermolecular hydrogen-bonding networks (purple dotted lines) involve coordinated water molecules and carboxylate groups of diphenate ligands from neighboring cluster units. Color codes as in Figure 1.

Structural Description of $[Co_2(dpa)_2(pyz)]_n$ (2)

Single crystal structure X-ray diffraction reveals that compound **2** (Figure 3) consists of dinuclear cobalt(II) units, each of which is symmetrically bridged by four carboxylate groups of four diphenate groups. Neighboring dinuclear units are interlinked via two diphenate ligands to form one-dimensional strands that can be described as double-helical chains along the *c* axis (Figure 4). These strands are interconnected by pyrazine molecules, which results in the formation of two-dimensional sheets (Figure 5). The asymmetric unit of **2** is displayed in Figure 3, selected bond lengths and angles are listed in Table 2, and a packing diagram is given in Figure S2 (see Supporting Information). The cobalt centers assume a square-based pyramidal NO_4 environment with four carboxylate oxygen atoms in the equatorial plane, with Co–O distances ranging from 1.989(5) to 2.043(5) Å. The apical position is occupied by the nitrogen atom of the pyrazine [Co1–N1 2.094(5) Å]. The Co···Co distance of 2.716(2) Å in the dinuclear units is in agreement with that in other discrete cobalt(II) dimers,[20a] but is significantly shorter than in the trinuclear complex **1** as well as in the related paddle-wheel chain $[Co_2(chdc)_2]_n$ (chdc = *trans*-1,2-cyclohexanedicarboxylate),[20b] where the intradimer Co···Co distance is 2.912(1) Å. Each dicarboxylate unit represents a tetradentate ligand and bridges two cobalt(II) centers through its carboxylate groups in a bis-monodentate fashion. Dinuclear unit pairs are linked by two dicarboxylic acids with the shortest distance between

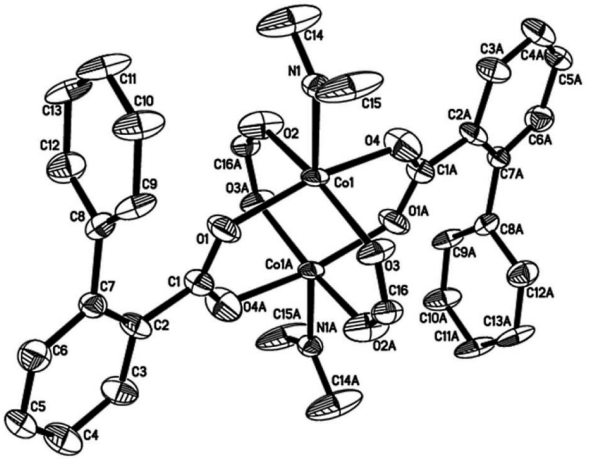

Figure 3. ORTEP plot of the dimeric asymmetric unit of compound **2**. "A" denotes the symmetry operation $-x + 1, -y, -z + 1$.

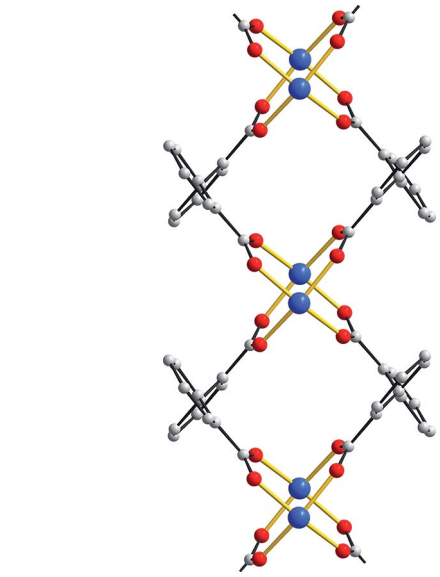

Figure 4. View of the double-helical chain along the *c* axis in compound **2**. Hydrogen atoms and pyrazine ligands have been omitted for clarity. Color code: Co: blue; O: red; C: gray.

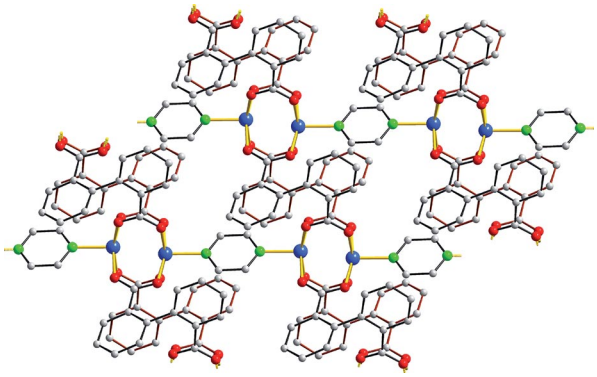

Figure 5. View of the two-dimensional sheet along the *b* axis in compound **2** showing the Co-dpa chains bridged by pyrazine ligands. Color code: Co: blue; O: red; N: green; C: gray. The front and rear diphenate groups in this perspective are indicated by black and brown bonds, respectively.

Table 2. Selected bond lengths [Å] and angles [°] in complex **2**.

Co1–O1	1.989(5)	O1–Co1–N1	101.1(2)
Co1–O2	2.043(5)	O2–Co1–N1	94.5(2)
Co1–O3	2.032(5)	O3–Co1–N1	99.4(2)
Co1–O4	2.009(6)	O3–Co1–O2	165.8(2)
Co1–N1	2.094(5)	O4–Co1–O2	87.2(3)
O1–Co1–O2	90.4(3)	O4–Co1–N1	93.1(2)
O1–Co1–O3	89.2(2)	O4–Co1–O3	89.8(2)
O1–Co1–O4	165.7(2)		

the dinuclear metal units of 6.403 Å. Note that the phenyl rings in the dpa^{2-} ligands are not coplanar and assume a dihedral angle between the ring planes of 76.87°.

Vibrational Spectroscopy

The FT-IR spectrum of compound **1** (Figure S3 in the Supporting Information) shows strong and broad bands in the regions 1598–1532 and 1403–1379 cm^{-1}, which correspond to the asymmetric and symmetric vibrations of the coordinated carboxylic groups of the dpa ligands, respectively. The presence of a strong band at 1704 cm^{-1} proves the existence of protonated uncoordinated carboxylic groups in **1**.[21,22] The asymmetric and symmetric vibrations of the coordinated carboxylic groups in **2** are found in the regions 1621–1561 and 1423–1397 cm^{-1}, respectively (Figure S4 in the Supporting Information).

Thermal Stability Studies

Thermogravimetric analyses for both complexes were performed under nitrogen in the temperature range 25–600 °C. For **1** (Figure S5 in the Supporting Information), the first weight loss step occurs at 230 °C and corresponds to the loss of two coordinated water molecules per formula unit (calcd. 2.7%; found 2.8%). The next step takes place at 315 °C, where loss of two 1-MeIm molecules and half a molecule of diphenate ligand can be observed (calcd. 21.3%; found 25.3%). The remaining carboxylate ligands decompose at 425 °C (calcd. 45.2%; found 48.9%). For **2** (Figure S6 in the Supporting Information), the decomposition of the amine ligands starts at 270 °C (calcd. 3.7%; found 3.4%). A further abrupt step at 450 °C corresponds to the loss of the remaining amine ligands and most of the diphenate ligands (calcd. 70.6%; found 68.3%). The decomposition of the carboxylic ligand is completed at 530 °C, and the corresponding mass loss (8.2%) agrees with the calculated value of 8.9%. All observed processes are endothermal.

Magnetic Properties

The magnetochemical interpretation of Co^{II} coordination complexes is frequently complicated by a multitude of factors, notably the fact that the free-ion ^4F ground term of Co^{II} is separated by the first excited state ^4P by more than 10^4 cm^{-1}.[23] In a weak ligand field with octahedral symmetry, the ^4F term splits into $^4T_1(F)$, $^4T_2$, and $^4A_2$ terms, while the ^4P term transforms into a $^4T_1(P)$ term. The $^4T_1(F)$ ground term for a high-spin Co^{II} center implies a significant contribution of the orbital momentum.[24] In 1971, Lines reported a statistical approximation for the analysis of the spin-spin coupling in dinuclear Co^{II} complexes with a $^4T_1$ ground term, although this was limited to the case of pure O_h symmetry.[25,26]

The magnetic data for compounds **1** and **2** were analyzed with the program CONDON[27] using a complete basis set (full d manifolds, i.e. 120 functions for Co^{II}) as a function of the applied field. Both factors are necessary to yield reliable information on the magnetic dipole orientation with respect to the local symmetry elements. CONDON takes into account the following single-ion effects: interelectronic repulsion (H_{ee}), spin-orbit coupling (H_{SB}), ligand-field effects (H_{LF}), and the applied field (H_{mag}). Generally, for a magnetically isolated 3 d^N metal ion in a ligand field (LF) environment in an external magnetic field B the Hamiltonian of the metal ion is represented by

$$\hat{H} = \underbrace{\sum_{i=1}^{N}\left[-\frac{\hbar^2}{2m_e}\nabla_i^2 + V(r_i)\right]}_{\hat{H}^{(0)}} + \underbrace{\sum_{i>j}^{N}\frac{e^2}{r_{ij}}}_{\hat{H}_{ee}} + \underbrace{\sum_{i=1}^{N}\zeta(r_i)\,\kappa\,\hat{\boldsymbol{l}}_i\cdot\hat{\boldsymbol{s}}_i}_{\hat{H}_{so}} + \underbrace{\sum_{i=1}^{N}\sum_{k=0}^{\infty}\left\{B_0^k C_0^k(i) + \sum_{q=2}^{k}\left[B_q^k\left(C_{-q}^k(i) + (-1)^q C_q^k(i)\right)\right]\right\}}_{\hat{H}_{LF}} + \underbrace{\sum_{i=1}^{N}\mu_B(\kappa\,\hat{\boldsymbol{l}}_i + 2\,\hat{\boldsymbol{s}}_i)\cdot\boldsymbol{B}}_{\hat{H}_{mag}}$$

While $H^{(0)}$ represents the energy in the central field approximation, H_{ee} and H_{so} represent the interelectronic repulsion and spin-orbit coupling (modified by the orbital reduction factor κ), respectively. The former is taken into account by the Slater–Condon parameters F^2 and F^4, and the latter by the one-electron spin-orbit coupling energy ζ. These parameters, as well as κ, are treated as constants in the following calculations. H_{LF} represents the electrostatic effect of the ligands within the framework of ligand-field theory based on the global parameters B_q^k. The summation is carried out over all N d electrons. The spherical tensors C_q^k are directly related to the spherical harmonics via $C_q^k = \sqrt{4\pi/(2k+1)}\,Y_q^k$; the real LF parameters B_q^k (in Wybourne notation)[28,29] are given by $A_q^k\langle r^k\rangle$ where A_q^k is a constant describing the charge distribution in the environment of the metal ion and $\langle r^k\rangle$ is the expectation value of the radial component of the wave function. For d electrons the terms in the expansion with $k \leq 4$ are nonzero, where all the terms with odd k values vanish (since only configurations containing equivalent electrons are considered). The point symmetry of the ligand field limits the values of k and q. If the spherically symmetric term $B_0^0 C_0^0$ (which causes no splitting) is ignored, only spherical tensors with $k \leq 4$ are relevant in cubic or tetragonal systems. The LF operator with reference to the fourfold rotation axis for the angular part of the wave function then reads

$$H_{LF}^{tet} = B_0^2\sum_{i=1}^{N}C_0^2(i) + B_0^4\sum_{i=1}^{N}C_0^4(i) + B_4^4\sum_{i=1}^{N}\left(C_4^4(i) + C_{-4}^4(i)\right)$$

In cubic systems, the LF parameter B_0^2 is zero and a fixed relation ($B_4^4\sqrt{5/14}B_0^4$) exists, consequently only the coefficient B_0^4 remains essential.

The matrix elements of $\hat{H}$, omitting $\hat{H}^0$, are evaluated by applying $\hat{H} = H_{ee} + H_{lf} + H_{so} + H_{mag}$ on the full basis of microstates. Diagonalization leads to the energies E_n and $|n\rangle$, where the latter serves as a basis for the applied mag-

netic field $\hat{H} = -\mu \cdot \boldsymbol{B}$. For specific field directions a, the energies $E_{n,a}$, are calculated and the quantities $\mu_{n,a} = -\partial E_{n,a}/\partial B_a$ are combined by Boltzmann statistics to give the macroscopic magnetization $M_{m,a}$ and the average molar susceptibility $\chi_{m,a} = \mu_0 M_{m,a}/B_a$ ($a = x, y, z$), $\chi_m = (\chi_x + \chi_y + \chi_z)/3$ and the effective Bohr magneton number $\mu_{eff} = 2.828\sqrt{\chi T}$ (CGS units) are obtained. An isotropic Heisenberg-type Hamiltonian $H_{ex} = -2J_{ex}\hat{S}_1 \cdot \hat{S}_2$ is used to describe exchange interactions between the magnetic centers, where a positive exchange energy (J_{ex}) corresponds to a ferromagnetic interaction.

The effective magnetic moment of the linear $\{Co_3\}$ complex **1** at 290 K is 4.72 μ_B per Co^{II} ion, significantly larger than the spin-only value of 3.87 μ_B and slightly smaller than the value resulting for both spin and orbital momentum: $\mu_{LS} = [L(L + 1) + 4S(S + 1)]^{1/2} = 5.20\ \mu_B$. For octahedral Co^{II} high-spin complexes ($S = 3/2$) in magnetically dilute systems we expected μ_{eff} values in the range 4–5[30] as a result of spin and first-order orbital contributions. The μ_{eff} value of compound **2** is 3.3 μ_B per Co^{II} ion, considerably lower than the spin-only value, thereby indicating antiferromagnetic exchange interactions between the Co^{II} centers.

Modeling the magnetic behavior therefore requires the ligand-field effect, spin-orbit coupling, and exchange coupling all be taken into account. The values for the spin-orbit coupling energy (ζ) and the reduction factor (κ) were chosen as 426 cm^{-1} and 0.8, respectively, and Racah parameters $B = 780$ and $C = 3680\ cm^{-1}$ were chosen on the basis of the optical spectra.[31]

Fitting Procedures for $[Co_3(dpa)_2(Hdpa)_2(1\text{-}MeIm)_2(H_2O)_2]$

Figure 6 shows the results of the magnetic measurement in the temperature range 2–100 K using molar susceptibility and effective Bohr magneton (μ_{eff}) vs. T plots. The magnetic moment increases with decreasing temperature below 20 K due to two primary factors, namely orbital momentum contributions and intramolecular ferromagnetic coupling between the three Co^{II} centers. Due to the molecular symmetry, the two exchange pathways between Co1 and Co2 and Co1 and Co2A (two μ-oxo and one μ-carboxylate group) are equivalent and characterized by a common exchange energy J_{ex}. We neglect intermolecular interactions between the neighboring clusters due to their large separation [d(Co···Co) = 5.712 Å]. The structure of **1** shows two different Co site symmetries. Thus, while for the central Co1 position the donor sites of the ligands form a near-perfect octahedral symmetry, the Co2/Co2A environments have (distorted) square-pyramidal symmetry. The ligand-field parameter B_4^4 was therefore employed for Co1, and B_0^2, B_0^4, and B_4^4 for Co2/Co2A.

The parameters J_{ex} and B_q^k were determined by minimizing the least-squares fit. The best fit for calculated and experimental χ_m values was found for $J_{ex} = 1.4\ cm^{-1}$, $B_0^2 = -33600\ cm^{-1}$, $B_0^4 = 7200\ cm^{-1}$, $B_4^4 = 20500\ cm^{-1}$ (Co2/Co2A), $B_0^4 = 8500\ cm^{-1}$ (Co1), and $SQ = 1.9\%$ (solid lines in Figure 6). Note that the dashed μ_{eff} vs. T plot in Figure 6 illustrates the single-ion contributions, namely the ligand-field effect. The ferromagnetic exchange between the Co1 and Co2/2A centers is interpreted to be caused primarily by the contributions of the Co–O1–Co (102.8°) and the Co–O8–Co (91.7°) bridges; ferromagnetic coupling has also been observed in a similar $\{Co_3\}$ structure, $[Co_3(phcina)_6(quin)_2]$ (see above).[19b]

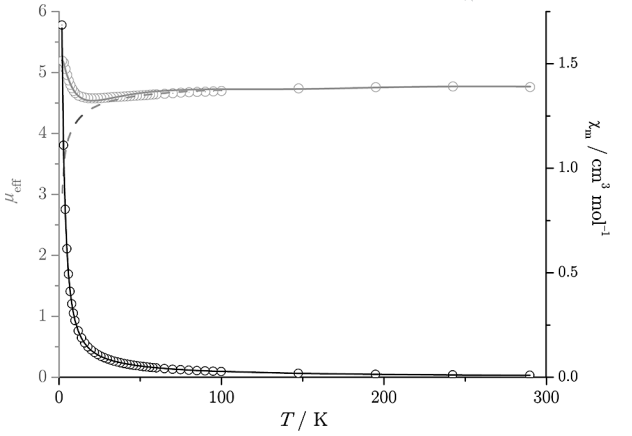

Figure 6. μ_{eff} vs. T (gray) and χ_m vs. T (black) plots for **1**, referenced to a single Co^{II} ion, at an applied field (B_0) of 0.1 T. Open circles: experimental data; solid lines: best fits for the employed model system. The dashed graph illustrates the effect of the ligand fields in absence of (weak ferromagnetic) exchange coupling.

Fitting Procedures for $[Co_2(dpa)_2(pyz)]_n$

Figure 7 displays the results of the magnetic susceptibility measurements in the temperature range 2–400 K as molar susceptibility (χ_m) vs. T plots. In the temperature range 400–350 K, χ_m has a value close to $6.61 \times 10^{-3}\ cm^3\,mol^{-1}$, which is significantly lower than the value expected for two magnetically uncoupled Co^{II} ions ($\mu_{eff} = 3.87$ for $g = 2.0$; spin-only value). The maximum in the χ_m vs. T plot (Figure 7) is characteristic for compounds displaying strong intramolecular antiferromagnetic coupling. At temperatures below 350 K, χ_m decreases continuously to reach a minimum of around $2.25 \times 10^{-3}\ cm^3\,mol^{-1}$ at 55 K. This value then increases again as the temperature is lowered further, which we attribute to paramagnetic impurities (monomeric Co^{II} species).

Three factors are responsible for the observed features, namely orbital momentum contributions, intramolecular antiferromagnetic coupling between the Co^{II} centers in the $\{Co_2\}$ subunits, and intermolecular interactions between the $\{Co_2\}$ subunits. While we describe the intramolecular interactions between the magnetic centers using an isotropic Heisenberg model (with $S_1 = S_2 = 3/2$), the multidimensional intermolecular exchange interactions between the dinuclear units are modeled using a phenomenological approach, the molecular field approximation

$$\chi_m^{-1} = \chi_m^{-1}(B,C,\varsigma,B_q^k,J_{ex}) - \lambda_{MF}$$

where χ_m denotes the susceptibility per Co^{II} ion and λ_{MF} the molecular field parameter. Positive and negative values

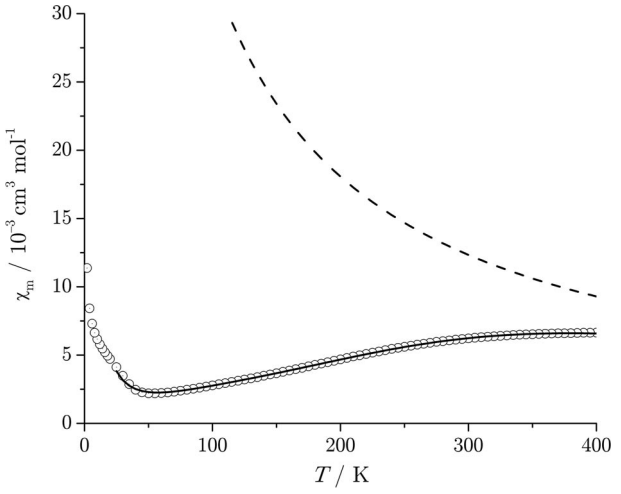

Figure 7. χ_m vs. T plots for **2**, referenced to a single Co^{II} ion, at an applied field (B_0) of 0.1 T. Open circles: experimental data; solid line: best fit; dashed graph: best fit in absence of intra- and intermolecular exchange interactions.

for λ_{MF} correlate with dominant ferromagnetic and antiferromagnetic interactions, respectively, between the dinuclear units.

The parameters J_{ex}, B_q^k (see above), and ρ (percentage of paramagnetic impurities) were determined by minimizing the susceptibility least-squares fit (T = 20–400 K). The best fit for calculated and experimental χ_m values was found for J_{ex} = –197 cm^{-1}, B_0^2 = –1360 cm^{-1}, B_0^4 = 3300 cm^{-1}, B_4^4 = –1900 cm^{-1}, λ_{MF} = 311 mol cm^{-3}, ρ = 0.5%, and SQ = 1.0%. As expected, exchange coupling between the Co sites of the dinuclear subunits is antiferromagnetic ($J_{ex} < 0$), but both a positive molecular field parameter λ_{MF} (indicating ferromagnetic interdimer coupling, primarily mediated by the pyrazine ligands) and a small paramagnetic impurity ρ are essential to reproduce the experimental susceptibility. As in Figure 6, the dashed line demonstrates the contribution for uncoupled Co^{II} ions without any exchange interactions.

Conclusions

New types of diphenate coordination compounds, namely the trinuclear complex $[Co_3(dpa)_2(Hdpa)_2(1\text{-}MeIm)_2(H_2O)_2]$ (**1**), which contains discrete $\{Co_3\}$ coordination clusters anchored in the solid-state lattice via a complex hydrogen bond network, and the two-dimensional coordination network $[Co_2(dpa)_2(pyz)]_n$ (**2**), which exhibits a double-helical connectivity, both of which illustrate the versatility of diphenic acid as a dicarboxylate ligand, have been obtained in the presence of appropriate N-donor ligands such as 1-methylimidazole or pyrazine. Magnetochemical analysis shows that the diphenate carboxylate groups can mediate both weak ferromagnetic as well as strong antiferromagnetic interaction between high-spin Co centers in the two described compounds, depending on their coordination mode, thus exemplifying the potential of the diphenate ligand for the rational design of molecule-based magnetic materials. Given the interesting finding that similar two-dimensional Co^{II} coordination networks exhibit single-chain magnet (SCM) features,[20b] we will continue to explore such Co^{II}-based coordination frameworks.

Experimental Section

Materials and Methods: All reagents were purchased from commercial sources and used without further purification. The IR spectra were recorded with a Perkin–Elmer Spectrum One spectrometer using KBr pellets in the region 4000–400 cm^{-1}.

TGA/DTA measurements were carried out with a Mettler Toledo TGA/SDTA851 instrument under dry N_2 (60 mL min^{-1}) at a heating rate of 10 K min^{-1}.

Synthesis of $[Co_3(dpa)_2(Hdpa)_2(1\text{-}MeIm)_2(H_2O)_2]$ (1): An aqueous solution of diphenic acid (0.24 g, 0.99 mmol) and 1-methylimidazole (0.15 mL) was added to an aqueous solution of $Co(O_2CMe)_2 \cdot 4H_2O$ (0.24 g, 0.96 mmol). This mixture (15 mL) was sealed in a Parr Teflon®-lined stainless reactor and heated at 160 °C for 16 h, then slowly cooled to room temperature over 24 h. Dark red crystals were collected by filtration, washed with water, and dried in a stream of argon; yield 34% (0.15 g). $C_{64}H_{50}Co_3N_4O_{18}$ (1339.9): calcd. C 57.35, H 3.76, N 4.18; found C 57.18, H 3.68, N 3.98. IR (KBr pellet): $\tilde{\nu}$ = 3445 (br), 3146 (w), 3062 (w), 1704 (s), 1598 (m), 1579 (s), 1556 (s), 1531 (s), 1403 (s), 1379 (s), 1237 (m), 1093 (w), 745 (m), 672 (m), 660 (m), 587 (w) cm^{-1}.

Synthesis of $[Co_2(dpa)_2(pyz)]_n$ (2): An aqueous solution of diphenic acid (0.24 g, 0.99 mmol), NaOH (0.08 g, 2 mmol), and pyrazine (0.08 g, 0.99 mmol) was added to an aqueous solution of $Co(O_2CMe)_2 \cdot 4H_2O$ (0.24 g, 0.96 mmol). This mixture (15 mL) was sealed in a Parr Teflon®-lined stainless reactor and heated at 160 °C for 16 h, after which the reaction system was slowly cooled to room temperature over 24 h. Dark brown crystals were collected by filtration, washed with water, and dried in a stream of argon; yield 65% (0.21 g). $C_{32}H_{20}Co_2N_2O_8$ (678.4): calcd. C 56.63, H 2.97, N 4.13; found C 56.58, H 2.75, N 3.88. IR (KBr pellet): $\tilde{\nu}$ = 3442 (br), 3060 (w), 1621 (s), 1589 (m), 1561 (w), 1423 (sh), 1397 (vs), 1289 (w), 1048 (w), 758 (m), 709 (m), 681 (m), 664 (sh), 477 (w), 462 (w) cm^{-1}.

Magnetic Measurements: Temperature-dependent susceptibility data for polycrystalline $[Co_3(dpa)_2(Hdpa)_2(1\text{-}MeIm)_2(H_2O)_2]$ (**1**) and $[Co_2(dpa)_2(pyz)]_n$ (**2**) were recorded using a Quantum Design MPMS-XL5 SQUID magnetometer in the temperature range 2.0–400 K at an applied field of 0.1 T. The data were corrected for the sample holder (Teflon® tubes) and the diamagnetic contributions of Co^{II} and the ligands [χ_{dia}(**1**) = -610×10^{-6} cm^3 mol^{-1}; χ_{dia}(**2**) = -305×10^{-6} cm^3 mol^{-1}].[32,33] The computational fitting quality parameter SQ is defined as

$$SQ = \sqrt{\sum_{i=1}^{n} ([\chi_{obs}(i) - \chi_{cal}(i)]/\chi_{obs}(i))^2}$$

X-ray Crystallography: A dark-red crystal of **1** with approximate dimensions $0.3 \times 0.25 \times 0.11$ mm^3 and a dark brown crystal of **2** with approximate dimensions $0.3 \times 0.2 \times 0.16$ mm^3 were mounted separately on a Bruker CCD-1000 diffractometer equipped with a Mo-K_α (λ = 0.71073 Å) radiation source. The crystal evaluation and data collection were performed at room temperature. After collection and integration, the data were corrected for Lorentz and polarization effects. The absorption correction was based on fitting

Table 3. Summary of single-crystal data collection and refinement details.

Compound	**1**	**2**
Empirical formula	$C_{64}H_{50}Co_3N_4O_{18}$	$C_{16}H_{10}CoNO_4$
Formula mass [g mol^{-1}]	1339.87	339.18
T [K]	298(2)	298(2)
Crystal system	monoclinic	triclinic
Space group	$P2_1/c$	$P\bar{1}$
a [Å]	10.1139(16)	7.315(3)
b [Å]	15.334(2)	9.457(4)
c [Å]	19.084(3)	11.203(5)
α [°]	90	83.489(8)
β [°]	97.326(3)	73.184(7)
γ [°]	90	68.945(6)
V [Å^3]	2935.5(8)	692.3(5)
Z	2	2
ρ [Mg m^{-3}]	1.516	1.627
μ [mm^{-1}]	0.917	1.257
Crystal size [mm]	0.30 × 0.25 × 0.11	0.30 × 0.20 × 0.16
θ range for data collection [°]	1.71–28.32	1.90–25.00
Index ranges	$-12 \le h \le 13$ $-19 \le k \le 20$ $-24 \le l \le 24$	$-8 \le h \le 8$ $-11 \le k \le 10$ $-13 \le l \le 13$
Reflections collected	26330	5081
Independent reflections	6957 [R(int) = 0.0383]	2400 [R(int) = 0.0343]
Completeness to θ	100.0%	98.0%
Data/restraints/parameters	6957/0/403	2400/0/199
Goodness-of-fit on F^2	1.049	1.042
Final R_1, wR_2	0.0351, 0.0772	0.0790, 0.2231
R indices (all data)	0.0594, 0.0889	0.0813, 0.2249
Largest difference peak/hole [e Å^{-3}]	0.404/–0.318	3.195/–0.929

a function to the empirical transmission surface, as sampled by multiple equivalent measurements using SADABS software.[34] The positions of heavy atoms were found by either direct or Patterson methods. The remaining atoms were located in an alternating series of least-squares cycles and difference Fourier maps. All non-hydrogen atoms were refined in full-matrix anisotropic mode using the SHELX suite of programs.[35] All hydrogen atoms were placed in the structure factor calculation at idealized positions and were allowed to ride on the neighboring atoms with relative isotropic displacement coefficients. Details of the crystal, data collection and refinement parameters are given in Table 3.

CCDC-708530 (for **1**) and -708531 (for **2**) contain the supplementary crystallographic data for this paper. These data can be obtained free of charge from The Cambridge Crystallographic Data Centre via www.ccdc.cam.ac.uk/data_request/cif.

Supporting Information (see also the footnote on the first page of this article): Packing diagrams for **1** (Figure S1) and **2** (Figure S2); IR spectra of **1** (Figure S3), and **2** (Figure S4); TGA and DTA curves for **1** (Figure S5) and **2** (Figure S6).

Acknowledgments

This work was supported by an RWTH Aachen University Seed Fund, the International Association for the promotion of cooperation with scientists from the New Independent States of the former Soviet Union (INTAS) (03-51-4532) and the Moldovan Research and Development Association/Civilian Research & Development Foundation (award no. MTFP-04-03).

[1] a) S. R. Batten, R. Robson, *Angew. Chem. Int. Ed.* **1998**, *37*, 1460–1494; b) P. J. Hagrman, D. Hagrman, J. Zubieta, *Angew. Chem. Int. Ed.* **1999**, *38*, 2638–2684; c) A. J. Blake, N. R. Champness, P. Hubberstey, W.-S. Li, M. A. Withersby, M. Schröder, *Coord. Chem. Rev.* **1999**, *183*, 117–138; d) R. Robson, *J. Chem. Soc., Dalton Trans.* **2000**, 3735–3744; e) M. Eddaoudi, D. B. Moler, H. Li, B. Chen, T. M. Reineke, M. O'Keeffe, O. M. Yaghi, *Acc. Chem. Res.* **2001**, *34*, 319–330; f) B. Moulton, M. J. Zaworotko, *Chem. Rev.* **2001**, *101*, 1629–1658; g) C. Janiak, *Dalton Trans.* **2003**, 2781–2804; h) O. M. Yaghi, M. O'Keeffe, N. W. Ockwig, H. K. Chae, M. Eddaoudi, J. Kim, *Nature* **2003**, *423*, 705–714; i) A. K. Cheetham, C. N. R. Rao, R. K. Feller, *Chem. Commun.* **2006**, 4780–4795; j) U. Müller, M. Schubert, F. Teich, H. Puetter, K. Schierle-Arndt, J. Pastre, *J. Mater. Chem.* **2006**, *16*, 626–636; k) A. Y. Robin, K. M. Fromm, *Coord. Chem. Rev.* **2006**, *250*, 2127–2157; l) M. Andruh, *Chem. Commun.* **2007**, 2565–2577; m) B. Wang, A. P. Cote, H. Furukawa, M. O'Keeffe, O. M. Yaghi, *Nature* **2008**, *453*, 207–211.

[2] M. A. Poray-Koshits, *Zh. Strukt. Khim.* **1980**, *21*, 146–180 (in Russian).

[3] a) N. Gerbeleu, Y. Simonov, G. Timco, P. Bourosh, J. Lipkowskii, S. Baka, D. Saburov, M. Mazus, *Russ. J. Inorg. Chem.* **1999**, *44*, 1191–1204; b) Y. A. Simonov, M. Gdaniec, I. G. Filippova, S. G. Baca, G. A. Timco, N. V. Gerbeleu, *Russ. J. Coord. Chem.* **2001**, *27*, 353–359; c) S. G. Baca, Y. A. Simonov, N. V. Gerbeleu, M. Gdaniec, P. N. Bourosh, G. A. Timco, *Polyhedron* **2001**, *20*, 831–837; d) S. G. Baca, I. G. Filippova, N. V. Gerbeleu, Y. A. Simonov, M. Gdaniec, G. A. Timco, O. A. Gherco, Y. L. Malaestean, *Inorg. Chim. Acta* **2003**, *344*, 109–116; e) S. G. Baca, Y. A. Simonov, M. Gdaniec, N. Gerbeleu, I. G. Filippova, G. A. Timco, *Inorg. Chem. Commun.* **2003**, *6*, 685–689; f) S. G. Baca, I. G. Filippova, O. A. Gherco, M. Gdaniec, Y. A. Simonov, N. V. Gerbeleu, P. Franz, R. Basler, S. Decurtins, *Inorg. Chim. Acta* **2004**, *357*, 3419–3429; g) S. G. Baca, S. T. Malinovskii, P. Franz, C. Ambrus, H. Stoeckli-Evans, N. Gerbeleu, S. Decurtins, *J. Solid State Chem.* **2004**, *177*, 2841–2849; h) S. G. Baca, I. G. Filippova, P. Franz, Ch. Ambrus, M. Gdaniec, H. Stoeckli-Evans, Y. A. Simonov, O. A. Gherco, T. Bejan, N. Gerbeleu, S. Decurtins, *Inorg. Chim. Acta* **2005**, *358*, 1762–

1770; i) S. G. Baca, I. G. Filippova, Ch. Ambrus, M. Gdaniec, Y. A. Simonov, N. Gerbeleu, O. A. Gherco, S. Decurtins, *Eur. J. Inorg. Chem.* **2005**, 3118–3130; j) S. G. Baca, M. T. Reetz, R. Goddard, I. G. Filippova, Y. A. Simonov, M. Gdaniec, N. Gerbeleu, *Polyhedron* **2006**, *25*, 1215–1222.
[4] J. Y. Lu, V. Schauss, *Inorg. Chem. Commun.* **2003**, *6*, 1332–1334.
[5] P. D. C. Dietzel, R. Blom, H. Fjellvang, *Dalton Trans.* **2006**, 586–593.
[6] R. Wang, Y. Zhou, Y. Sun, D. Yuan, L. Han, B. Lou, B. Wu, M. Hong, *Cryst. Growth Des.* **2005**, *5*, 251–256.
[7] a) J.-M. Rueff, S. Pillet, N. Claiser, G. Bonaventure, M. Souhassou, P. Rabu, *Eur. J. Inorg. Chem.* **2002**, 895–900; b) H. Kumagai, K. Inoue, M. Kurmoo, *Bull. Chem. Soc. Jpn.* **2002**, *75*, 1283–1289.
[8] J.-M. Rueff, S. Pillet, G. Bonaventure, M. Souhassou, P. Rabu, *Eur. J. Inorg. Chem.* **2003**, 4173–4178.
[9] A. Thirumurugan, S. K. Pati, M. A. Green, S. Natarajan, *J. Mater. Chem.* **2003**, *13*, 2937–2941.
[10] Y.-B. Wang, X.-J. Zheng, W.-J. Zhuang, L.-P. Jin, *Eur. J. Inorg. Chem.* **2003**, 1355–1360.
[11] R. Wang, Y. Gong, L. Han, D. Yuan, B. Lou, B. Wu, M. Hong, *J. Mol. Struct.* **2006**, *784*, 1–6.
[12] R. Wang, F. Jiang, L. Han, Y. Gong, Y. Zhou, M. Hong, *J. Mol. Struct.* **2004**, *699*, 79–84.
[13] R. Wang, L. Han, Y. Sun, Y. Gong, D. Yuan, M. Hong, *J. Mol. Struct.* **2004**, *694*, 79–83.
[14] P.-X. Yin, J. Zhang, J.-K. Cheng, Z.-J. Li, Y.-G. Yao, *Inorg. Chem. Commun.* **2006**, *9*, 541–543.
[15] R. Wang, M. Hong, J. Luo, R. Cao, J. Weng, *Chem. Commun.* **2003**, 1018–1019.
[16] P.-X. Yin, J. Zhang, Z.-J. Li, Y.-Y. Qin, J.-K. Cheng, Y.-G. Yao, *Inorg. Chem. Commun.* **2008**, *11*, 134–137.
[17] L. Du, R. Fang, Q. Zhao, *Acta Crystallogr., Sect. E* **2007**, *63*, m1439–m1431.
[18] J. Gao, S. Ma, Ch. Jin, D. Liao, *Polyhedron* **1996**, *15*, 2633–2639.
[19] a) J. Catterick, M. B. Hursthouse, D. B. New, P. Thornton, *J. Chem. Soc., Chem. Commun.* **1974**, 843–844; b) Y. Oka, K. Inoue, *Chem. Lett.* **2004**, *33*, 402–403.
[20] a) N. Benbellat, K. S. Gavrilenko, Y. L. Gal, O. Cador, S. Golhen, A. Gouasmia, J.-M. Fabre, L. Ouahab, *Inorg. Chem.* **2006**, *45*, 10440–10442; b) Y.-Z. Zheng, M.-L. Tong, W.-X. Zhang, X.-M. Chen, *Angew. Chem. Int. Ed.* **2006**, *45*, 6310–6314.
[21] K. Nakamoto, *Infrared and Raman Spectra of Inorganic and Coordination Compounds*, Wiley, New York, **1986**, p. 230.
[22] R. C. Mehrota, R. Bohra, *Metal Carboxylates*, Academic Press, New York, **1983**, p. 47.
[23] a) B. N. Figgs, M. A. Hitchman, *Ligand-Field Theory and its Applications*, Wiley-VCH, New York, **2000**; b) C. J. Ballhausen, *Introduction to Ligand Field Theory*, McGraw-Hill, New York, **1962**.
[24] O. Kahn, *Molecular Magnetism*, VCH Publishers, New York, **1993**.
[25] M. E. Lines, *Phys. Rev.* **1963**, *131*, 546–555.
[26] M. E. Lines, *J. Chem. Phys.* **1971**, *55*, 2977–2984.
[27] H. Schilder, H. Lueken, *J. Magn. Magn. Mater.* **2004**, *281*, 17–26.
[28] B. G. Wybourne, in *Spectroscopic Properties of Rare Earths*, Wiley, New York, London, Sydney **1965**.
[29] C. Görller-Walrand, K. Binnemans, in *Handbook on the Physics and Chemistry of Rare Earths* (Eds.: K. A. Gschneidner Jr., L. Eyring), Elsevier, Amsterdam, **1996**, vol. 23, Ch. 155, p. 121.
[30] E. König, S. Kremer, in *Magnetism Diagrams for Transition Metal Ions*, Plenum Press, New York, London, **1979**, pp. 305–320.
[31] A. B. P. Lever, in *Inorganic Electronic Spectroscopy*, Elsevier, Amsterdam, **1984**, pp. 317–333.
[32] W. Haberditzl, *Angew. Chem.* **1966**, *78*, 277–288.
[33] H. Lueken, *Magnetochemie*, Teubner, Stuttgart, **1999**, pp. 426–427.
[34] R. H. Blessing, *Acta Crystallogr., Sect. A* **1995**, *51*, 33–38.
[35] All software and sources of the scattering factors are contained in the SHELXTL (version 5.1) program library (G. Sheldrick, Bruker Analytical X-ray Systems, Madison, WI).

Received: November 21, 2008
Published Online: February 5, 2009

